# CMS RPC system operation and performance during LHC Run II data-taking

CMS Collaboration

June 22, 2019

**Abstract**

Resistive Plate Chambers (RPC) are one of the dedicated systems in CMS, used to measure and trigger on Muons. RPC system coverers both barrel and forward region to pseudo-rapidities up to $|\eta| < 1.9$. The performance of RPC system is studied using proton-proton collision data at center-of-mass energy $\sqrt{s} = 13\ TeV$, collected at the LHC during the full duration of Run 2 (from 2015 to 2018). The measured performance parameters, including spatial resolution, efficiency, and timing, are found to meet all design specifications, despite the more challenging running conditions during Run 2.

## Contents



## 1 Introduction

The Compact Muon Solenoid (CMS) is an experiment with a general-purpose detector at the Large Hadron Collider (LHC). CMS has strong physics program primarily to extend our understanding of the early Universe and the standard model of elementary particles. Since many of signatures of physics in interests include muons in the final states, CMS has

a design concept of high quality muon reconstruction over a board range of kinematic parameters. CMS detector is organized with a classical layout with an inner tracking detector at the innermost part, followed by Electromagnetic and Hadronic Calorimeters, located in a superconducting solenoid which produces strong magnetic field at 3.8 Tesla. In the outermost part of CMS, three types of muon detectors, Drift Tubes (DT), Cathode Strip Chambers (CSC) and Resistive Plate Chambers (RPC) are installed in the iron yoke, to enable muon triggering and reconstruction.

Run-1 of LHC finished in 2012. Experimental data of about 20 $fb^{-1}$ have been collected at center-of-mass energy 7 and 8 TeV. During the first long shutdown period (LS1, $2013-2014$), significant improvements were made by CMS, in order to prepare for the roughly doubled with respect to Run-1 collision energy of 13 TeV and higher instantaneous luminosity, reaching $2 \times 10^{34} cm^{-2} s^{-1}$. During LS1, the CMS muon system was upgraded with 144 newly installed RPC chambers on the fourth forward endcap (closing parts of CMS) stations (RE4), in order to ensure and enhance the muon trigger efficiency. As a result of the improvements to the muon detector and reconstruction algorithms, and in spite of the higher instantaneous luminosity, the performance of the muon detector and reconstruction is as good as or better than Run-1. Moreover, all performance parameters remain well within the design specifications of the CMS muon detector.

The present paper describes the performance of the Run-2 ($2015-2018$) CMS RPC system in terms of detector efficiency, cluster size, hit resolutions, currents, backgrounds and trigger efficiency. It is based on proton-proton collision data collected during Run-2 at $\sqrt{s} = 13\,\text{TeV}$ with instantaneous luminosity up to $2 \times 34\,\text{cm}^{-2}\,\text{s}^{-1}$.

# 2 The CMS RPC system and its operation

## 2.1 CMS RPC system during the Run-2

Three types of gaseous detector technologies are used in the CMS to reconstruct and identify muons. On figure 1 the quadrant part of the CMS detector is shown. Precise standalone muon tracking relies on the DT in the Barrel region (pseudo-rapidity $|\eta| < 1.2$) and the CSC the Endcap region ($1.2 < |\eta| < 2.4$). The RPC can provide fast and accurate assignment of particle collision (bunch crossing) at the triggering level, in both Barrel and Endcap regions up to $|\eta| < 1.8$.

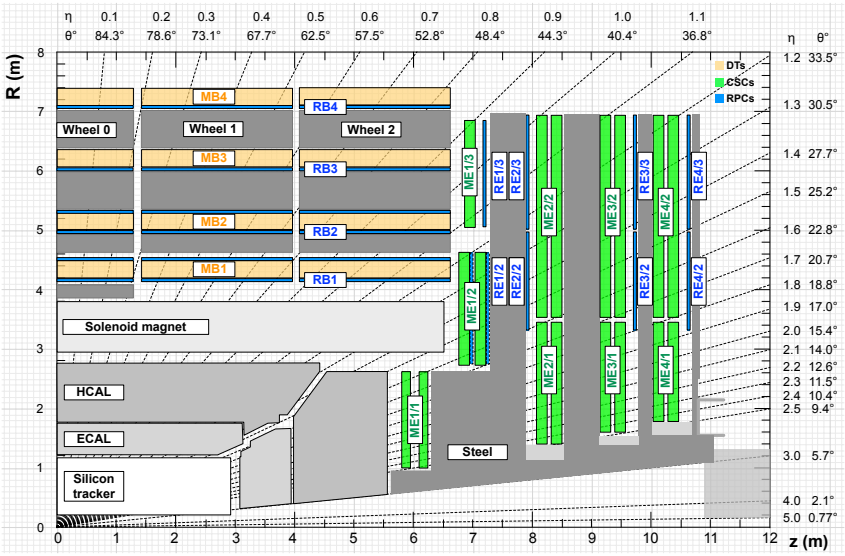


Figure 1: Quadrant figure of the CMS detector. The RPC chambers are shown in blue.

The Barrel region is divided into 5 separate wheels along the beam axis (named W$\pm$2, W$\pm$1 and W0). RPCs in each wheels are organized by 6 layers. The first four layers are attached before and after the DTs in the first two stations (named RB1in, RB1out, RB2in,

RB2out, RB3, RB4). In the Endcaps, there are 4 disks both in the forward and backward directions (named RE±4, RE±3, RE±2, RE±1). In the $\phi$ direction, each wheel is divided into 12 sectors while every disk into 36 sectors. In total there are 1056 RPC chambers, covering an area of about 3950 $m^2$, equipped with about 123 688 readout strips. The geometry of the RPC strips is mainly driven by the need to have the trigger adjustable on different $p_T$ muons. Therefore, the strips are aligned along the $\eta$ and their shapes are rectangular in the Barrels while they are trapezoidal in the Endcaps.

The CMS RPCs are equipped with two 2 mm gas gaps width each and copper readout in between. High voltage (HV) is applied to the electrodes which are made out of phenolic resin (called bakelite), and whose bulk resistivity is in the range of $2 - 5\ 10^{10}\ \Omega$ cm. They operate in avalanche mode. Conditions of the CMS RPCs are calibrated to ensure the expected time resolution of $\approx 2$ ns at rates of the order of 10 kHz $cm^{-2}$, with the number of signal strips by a muon (Cluster size) at $2 \sim 3$. More details about the CMS muon system can be found in reference [1].

## 2.2 Chamber gas issues during the operation

The CMS RPCs operate with a a gas mixture of 95.2% $C_2H_2F_4$, 4.5% $iC_4H_{10}$ and 0.3% $SF_6$. Fig 2 shows the Isobutane concentration level in the RPC system during the period $2016 - 2018$. The two red lines on the plot mark the limits for optimal performance of the CMS RPCs. With green color is given the Isobutane concentration from the mixer. The gas coming from the system before purifier 2 is shown with red color. The blue dots represent the gas going back to the system. As might be seen from the plot, in 2016 the Isobutane concentration in the RPC gas working mixture was higher. The reason was a problem with the mass flow controller. Similar problem was observed also in the beginning of the 2018. Higher Isobutane concentration led to an increase of the clusters size (number of fired adjacent strips) ans it was taken into account during the HV working points evaluation. More details about the calibrations will be shown in the next section of this document. The most serious operational problem during the Run-2 were the spotted gas leaks, caused mainly by the broken connectors.In order to reduce the gas leak flow, 37 leaky chambers have been switched off, resulting in a 3.5% inactive channels of the entire system. During the LS2 (Long Shutdown 2) period is scheduled a strong program aiming to repair as many leaky chambers as possible.


Figure 2: Isobutane concentration level in RPC system in $2016 - 2017$

# 3 Data Analysis approaches

## 3.1 Segment extrapolation method

Studying the performance of a big detector system requires different analysis approaches, including permanent monitoring of main operational quantities as currents, high voltage, gas composition, ambient environment etc. related to the operational capability of the chambers. Such parameters have been monitored through the detector control system and have been stored in a dedicated data base. A dedicated tool have been developed in order to extract this information for further analyses. From the other side the participation of the system in global data taking, its contribution to the L1 (level one trigger system) and muon reconstruction have been carefully analyzed. CMS data collected in proton-proton collisions and cosmics runs have been used for an evaluation of the chamber hit efficiency, cluster size (size of the formed clusters of adjacent fired strips ), time and space resolution, and muon trigger efficiency as well. Two different approaches have been used to study the RPC hit efficiency - the segment extrapolation method (cite Camilo) and extrapolations from the inner tracker detector (cite T&P). The Segment extrapolation method explores standalone muons, reconstructed only in the muon system and thus ensure enough statistics for the run based analysis. The redundancy of the muon system allows to explore the information for the nearest muon detectors for RPC efficiency calculations. In order to avoid bias the standalone muon reconstruction was done without using the RPC information. The segments built in the nearest DT (in the barrel) or CSC chamber (in the endcap) have been extrapolated to the RPC plane, where the segments have been selected to belong to a standalone muon track. The reconstructed RPC clusters (RPC rechits) have been matched to the extrapolated points, where the coincidence were searched in the vicinity of 2 strips. The efficiency for every RPC roll (eta partition) has been calculated as the ratio between the matched RPC hits and the extrapolated ones. Runs with duration more than half an hour have been considered as a good for analysis in order to ensure enough statistics for the entire detector. The segment extrapolation method is in use since it development from Run-1 up to the end of Run-2.

## 3.2 Tracker tracks extrapolation and T&P

However, due to the geometry constrains or temporary local problems with the other muon detectors, some RPC chambers might remain "non-illuminated" and efficiency calculations for them are not possible in such cases. These are mainly the RPCs installed in the most forward region $|\eta| > 1.6$ and some chambers of the forth barrel station. Because of this, another method has been the developed. The charged particles tracks reconstructed in the inner silicon tracker are extrapolated to the muon chambers and have been tagged by the RPC rechits. The newly built objects are called RPC Muons (cite rpc muons reco - Min Suck) and do not use an information from the DT or CSC system. Thus the tracker tracks extrapolation to the RPC system is an independent from the otehr muon reconstruction algorithms and might be used for non-biased efficiency calculations. In order to ensure a good analysis quality the muon sample has been selected thanks to the so called Tag and Probe (T&P) method. Both the methods have been compared and show consistent results. A small systematic difference of $0.5 - 1.6\,\%$ is observed where the T&P method results in a bit higher efficiency. The T&P method is closer to the analysis approaches used by the other muon detectors, and thus allows to develop a common base for comparison and studies of the entire muon system. However the T&P method is highly statistically dependent and require analysis of the data collected in larger time periods.

# 4 RPC system performance and calibration

## 4.1 Efficiency

The two most important criterion for the RPC system performance are hit efficiency and cluster size (CLS). In Figure 3 the history of RPC hit efficiency and CLS are shown. The

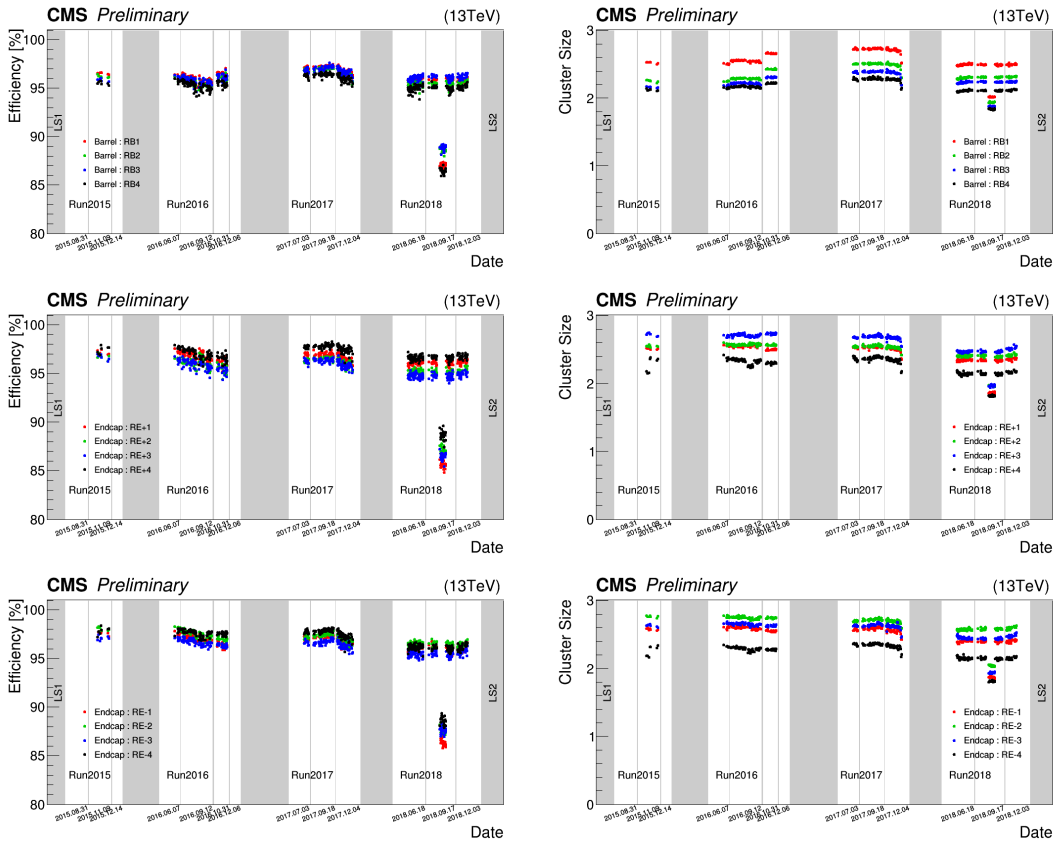


Figure 3: RPC hit efficiency and cluster size (CLS) history during entire Run-2. The top plots represent the barrel station, the plots in the middle – positive endcap and the bottom plots - the negative endcap. The drop observed in a short period of the 2018 is caused by a wrong on-line configuration settings and lower HV working points.

results are obtained with T&P method and in order to ensure a good statistics the hits, collected in a detector part under study, over one LHC fill are integrated. Thus every point on the figure represents a particular LHC fill. The system performance remain stable and depends mainly on the hardware calibration and changes in the working gas mixture composition.In 2016, because of higher Isobutane concentration (5.3%), efficiency was lower as the HV working points (WP) were not changed to compensate the wrong gas mixture. After the deployment of the new WP in September 2016, the efficiency increased slightly by 1% and cluster size increased sharply. Gas concentration was back at 4.5% in 2017 but the WP were not changed. The efficiency remained unchanged (running in the plateau of the sigmoid curve), however a new increase of the cluster size have been observed. New WP have been deployed by end of 2017, which led to a slight decrease of the efficiency but sensible reduction of the cluster size. The drop in the short period of 2018 data taking is caused by a human error and loaded lower HV working points.

In Figure 4, RPC efficiency as a function on the integrated luminosity is shown. As it might be seen from the plots the system performance remains stable and no degradation of it is observed up to the 150 $fb^{-1}$. Hence as a main criteria for a system ageing, the number of chambers switched Off or put to operate in single gap mode have been considered. In Figure 5 the hit efficiency per every RPC roll is shown. Black areas coressponf to the chambers switched Off because of the gas leak in the barrel and low voltage problems in the endcap.

Despite all the faced problems, the overall performance of the RPC system during the entire Run-2 is stable. The plots in Figure 6 show a comparison between the overall performance in all 4 years of data taking. The efficiency measured in the different years is stable and more than 95 %, following the CMS requirements.

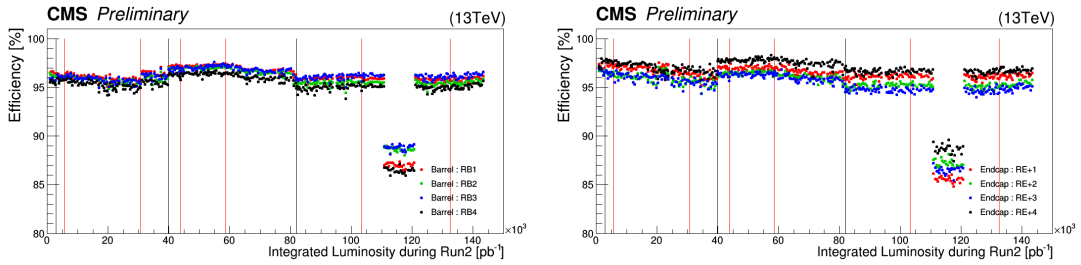


Figure 4: RPC hit efficiency and cluster size (CLS) history during Run-2 as a function on the integrated luminosity. Plot on the left represents the barrel stations, and on the right - the stations in the positive endcap. Results for the negative part are similar and thus not shown here. The drop observed in a short period of the 2018 is caused by a wrong on-line configuration settings and lower HV working points.

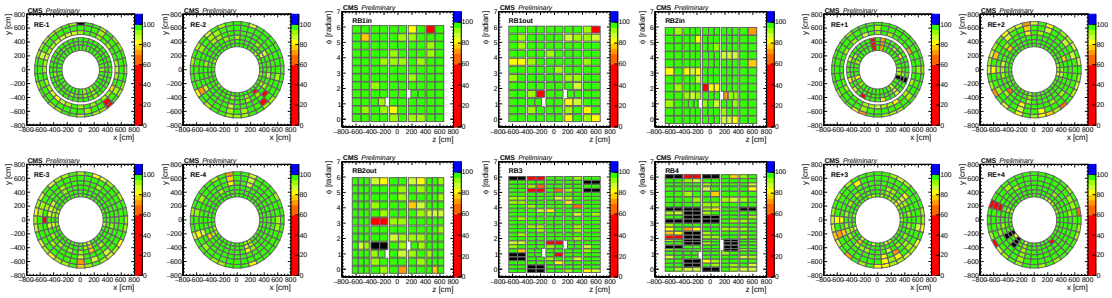

Figure 5: Overall efficiency of RPC rolls during 2018 pp data taking. Black area corresponds to the off-chambers.

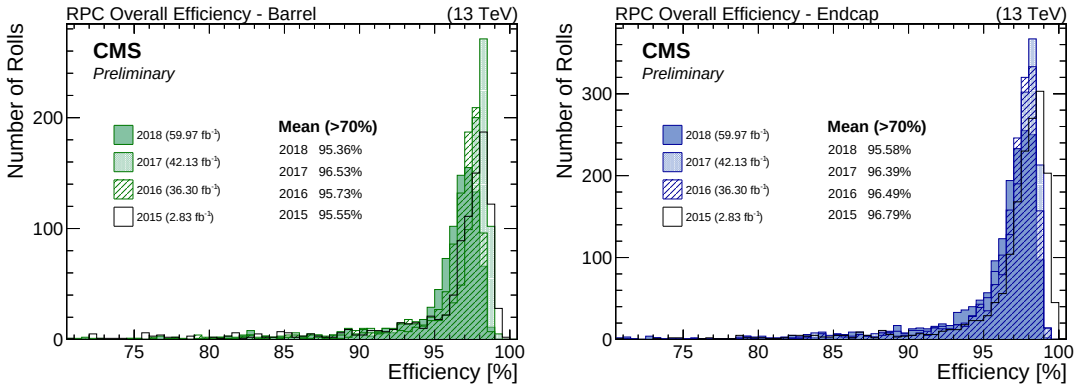


Figure 6: Comparison of overall efficiency distribution in 2015-2018 pp data taking.

## 4.2 Time resolution

The CMS RPCs are used mainly as trigger detectors. Thanks to the time resolution of about 2 ns they can provide fast identification and bunch-crossing assignment of the measured particle. The RPC time information is used in all muon track finders, explained in 6. The distributions of the bunch-crossing (BX) assigned numbers to the RPC hits from muons, measured in 2018 proton-proton collisions are shown in Figure 7. Muons from primary collisions are triggered in the central (zero) BX window. Small fraction ($\leq$ 1%) of post-collision hits is a reason for the contribution in the first BX window after the central one.

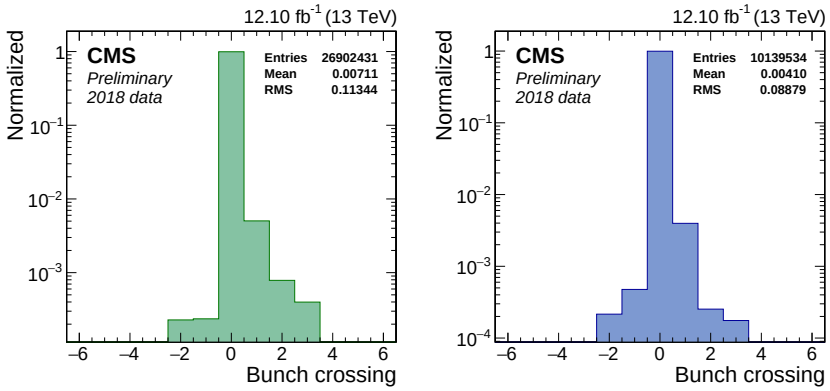


Figure 7: RPC bunch crossing distribution in the barrel (on the left) and endcap (on the right).

## 4.3 Spatial resolution

The RPC hits positions are used by the trigger algorithms and in addition they add complementary information to the muon reconstruction ensuring the redundancy ot he entire muon system. The position of the hit is measured in the gravity center of the formed cluster. The spatial resolution has been studied with segment extrapolation method. The residuals are calculated as distance between DT (CSC)-segment extrapolation and the closest RPC hit. The residuals depend on the cluster size and vary for the different stations depending on the strip pitch. Gaussian fit is performed on each distribution and the measured standard deviations are between 0.9 and 1.4 cm for the stations with the smallest and largest strip pitch respectively.

## 4.4 Working point calibration

RPCs are gaseous detectors in the gas amplification depends form the pressure and temperature. In order to ensure a smooth and stable operations the applied voltage ($HV_{app}$) is controlled and corrected automatically by the detector control system in order to keep the detector effective voltage ($HV_{eff}$) as constant as possible. The corrections is given by:

$$\mathrm{HV_{app}} = \mathrm{HV_{eff}}\,(1 - \alpha + \alpha\,\frac{P}{P_0}\,\frac{T_0}{T}), \tag{1}$$

where $P$ and $T$ are the pressure and temperature in the CMS cavern and $P_0 = 965\,\mathrm{mbar}$ and $T_0 = 293\,\mathrm{K}$ are their reference values. The parameter $\alpha$ is used to minimaze the overcorrection effects and it's value is chosen to be 0.8 [2]. The environmental temperature in the experimental cavern is quite stable and the themperature correction is negligible.

The optimal operating voltage of each chamber is estimated using a special calibration procedure and taking several calibration runs, called HV scans. Turing the HV scan the date is taken changing equidistantly the applied voltage from 8.8 to 9.8 kV. To avoid possible bias RPCs are not used in the trigger during these runs and the events are triggered by DTs and CSCs. Muons trajectories are build using the CMS standard muon reconstruction

[3]. The chamber efficiency is estimated for each applied voltage and efficiency vs voltage dependence is fitted by sigmoid:

$$\varepsilon = \frac{\varepsilon_{\max}}{1 + \exp(-\lambda(\mathrm{HV}_{\mathrm{eff}} - \mathrm{HV}_{50\%}))}, \tag{2}$$

where $\lambda$ characterizes the slope of the sigmoid at the inflection point, $\varepsilon_{\max}$ represents the asymptotic efficiency for HV $\rightarrow \infty$, and $\mathrm{HV}_{50\%}$ is the inflection point for which 50% of $\varepsilon_{\max}$ is reached. The optimal working point (WP) for each chamber is determined by interpolating the $\varepsilon$ distribution using the fit parameters in Eq. 2 and computing the HVat 95% ($\mathrm{HV}_{95\%}$) of the $\varepsilon_{\max}$ reached. Then the WP for each chamber is defined as $\mathrm{HV}_{95\%}+$ 100 V or 120 V for barrel or endcap chambers, respectively. The difference allows barrel and endcap to provide similar global efficiency [4, 5].

Since each HV channel supplies a maximum of two chambers mainly in the endcap. The resulting WPs applied in the HV channel are averaged for chambers belonging to the same channel supplier.

The RPC chambers without providing proper data required for the present method are excluded. They are the chambers whose efficiency data obtained from the tracker detectors are missing. The chambers operated in a single-gap mode because of gas leak or HVproblem are also excluded from the analysis.

During the LS1 maintenance period the HV scans in 2013 and 2014 were not performed, in 2015 the scan was omitted to avoid introducing unknown bias to the study due to the missing magnetic field during the data taking. In the Fig. 8, it is shown the average of WP for barrel and endcap in the second active period of the LHC, and the expected efficiency at WP. It has been variations in the mixture of gas composition inside of the RPC chambers which affect the WP values, as well as, the luminosity conditions in the data taking, however high efficiency is kept.

# 5 Radiation background studies

## 5.1 Background

Background radiation levels play a decisive role with respect to the performance of the existing detector, as well as to the design of the upgraded Muon system for the High Luminosity running of the LHC (HL-LHC) [6]. Any background source, including low energy neutrons or photons, electrons and positrons, punch-through hadrons, low momentum primary and secondary muons, and beam-induced background (particles produced in the interaction of the beams with collimators, residual gas, and beam pipe components), could affect the muon trigger performance and pattern recognition of muon tracks. In particular, spurious hits due to noise or to radiation background could promote low transverse-momentum muons to higher momentum. In addition, excessive radiation levels can cause aging of the detectors. Furthermore, the expected radiation levels during the HL-LHC can contribute to drive the choice of the most suitable technology for the detector upgrade. Reliable estimates of the expected hit rates are therefore essential [7].

### 5.1.1 RPC Hit Rate Definition

There are three main components contributing to the RPC hit rates - muon events (from primary collisions and from cosmics as well), intrinsic noise of the strips, and radiation background, where the main contribution is caused by the radiation background. There are two main sources of the it - particles from primary collisions and from their secondary interactions, and neutron induced background in the cavern. Detector layers installed closer to the beam pipe and hence to the primary interactions are affected mainly by the prompt radiation component, while the outermost stations are affected mainly by the cavern background. RPC hit rates are measured at the strip level using the incremental counts of the RPC trigger link-boards. No trigger selection is applied at this stage, resulting in an inclusive measurement of the radiation background rates. For every particular run, the total number of counts, for the detector region under study, has been integrated and normalized to the run duration time and the area of active strips.

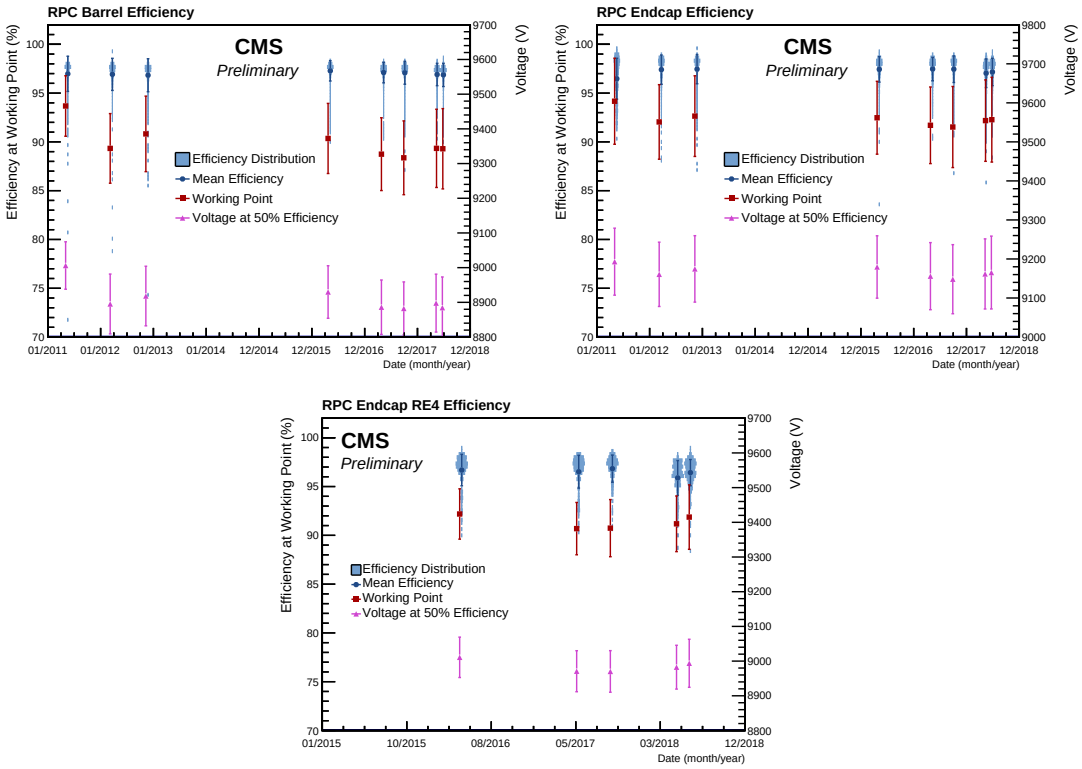


Figure 8: Efficiency distribution for each HV scan with their standard deviations: The plot represents the working point (WP) evolution, the efficiency at the working point evolution and the Voltage at 50%. The efficiency at WP distributions have been presented with a light blue color. With a blue, full circle is presented the mean efficiency at WP for each of the HV scans. By red, full squares is represented the mean of the working point distribution for each HV scan with their Standard deviations. In magenta, full triangles represent the mean of the voltage at 50%. A shift of around 40 V to lower values has been observed in 2017 with respect to 2016, caused by the higher Isobutane concentration in the CMS RPC standard gas mixture during 2016. Lowering of the HV WP does not affect the chamber efficiency as seen on the plot since chambers are already working at efficiecny plateau. The top plots depict the barrel and first three endcap stations, while the bottom one represents the forth endcap stations, added to the system after Run-1.

### 5.1.2 Luminosity Dependence

A linear dependence of the RPC hit rates on the instantaneous luminosity is measured during the entire Run-2 of data taking. This dependence is stable within the fills, though the slope of it may depends on the particular LHC conditions. Because of this, stable runs with number of colliding bunches more than 600 and comparable run durations have been selected for the study. The instantaneous luminosity has been obtained using the official CMS tools. Averaged hit rates values per barrel and endcap stations, measured in 2018 proton-proton collisions are shown on Figure 9. As it might be seen from the plot highest rates are measured for the first barrel station (RB1), caused by the prompt particles, and for the outermost stations both in the central and endcap parts (RB4, RE+4, RE-4), where the forth endcap stations are the mostly affected ones.

### 5.1.3 Cavern background

RPC system covers both the barrel and endcap parts of the detector. CMS explores cylindrical geometry conception and it is worth to recoil that pseudorapidity is a function both on the radius (distance to the beam pipe) and Z (distance from the interaction point along

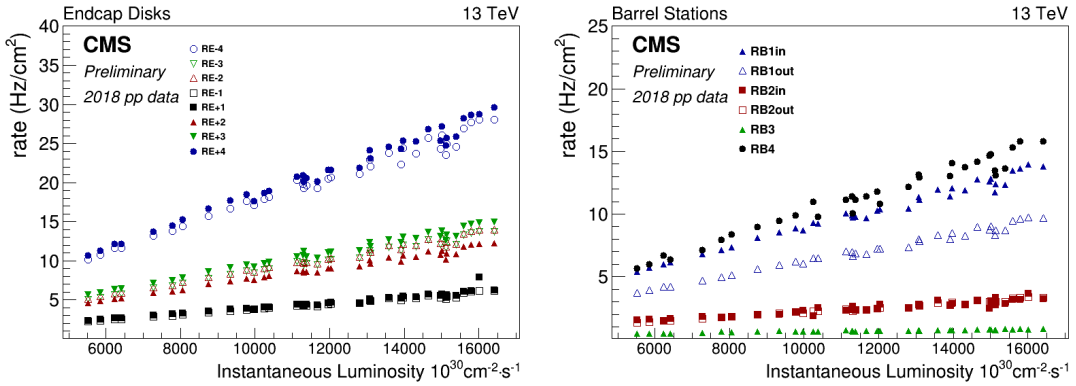


Figure 9: The RPC hit rate as a function of instantaneous luminosity for the Endcap (top left), Barrel Wheels (top right), and Barrel Stations (bottom) is shown in the figure.

the beam pipe). The rate distributions as a function of pseudorapidity are shown in Figure 10. For the barrel layers, the rates are averaged over $\phi$ for all the chambers installed at same radii, while in the endcap part the average values are taken for the chambers installed at same Z. The rates are calculated at instantaneous luminosity of $1.5 \times 10^{34} s^{-1}$ cm$^{-2}$s$^{-1}$ and have been compared to the MC prediction of separate studies with FLUKA. The comparison shows good agreement between the MC and the experimentally measured values in the barrel and small difference in the endcap part of factor of 2. Nevertheless the distributions show coherent trends. As might be seen from the plots the background increases with absolute value of $\eta$ with the only exception in the first stations. The leak from the gap in the HCAL affects mainly the muon chambers from the first barrel station of the outermost wheels and less the chambers form the first endcap stations.

In Figure 11 rate distributions for all the endcap chambers as a function of $\phi$ are shown. The rates are calculated from the linear fit at instantaneous luminosity of $1.5 \times 10^{34} s^{-1}$ cm$^{-2}$s$^{-1}$. As it might be seen from the plot the cavern background is not uniformly distributed and affects mainly the top sectors (around 90 deg) of the forth stations and it is lower for the sectors near to the bottom of the cavern. The reason is the neutron gas in the cavern and also the background leaks from the gaps of the rotating shielding. The linear dependencies have been extrapolated up to the instantaneous luminosity of $5 \times 10^{34} s^{-1}$ cm$^{-2}$s$^{-1}$ in order to predict the expected RPC rates at HL-LHC (High Luminosity LHC) conditions. The predicted rates as a function of $\phi$ are shown on the same figure. As it shown on the plot the maximum expected rate is about 200 Hz/cm$^2$ and this is the maximum expected value for the entire present RPC system.

# 6 RPC System in CMS Level-1 Muon Trigger

In 2016 and 2017, CMS performed an upgrade of its Level-1 (L1) muon trigger system [8] moving from a muon detector-based scheme to a geometry-based system. The three detector track finders (TF) – DTTF, RPCTF and CSCTF – have been replaced by three track finders covering each a specific pseudo-rapidity region: the barrel muon track finder (BMTF) covering $|\eta| < 0.83$, the overlap muon track finder (OMTF) covering $0.83 < |\eta| < 1.24$ and the endcap muon track finder (EMTF) covering $|\eta| > 1.24$.

Compared to the legacy system, the upgraded architecture allows concurrent access to information from several muon detectors at an earlier stage in the trigger chain ensuring a better usage of the muon system redundancy. The BMTF uses DT and RPC information, the EMTF relies on CSC and RPC data while OMTF can use informations from all three detectors. This upgrade of the L1 muon trigger lead to an important rate reduction over the whole eta range while keeping similar efficiency as shown on Fig. 12 [9]. Note that this performance gain also comes from other aspects of the L1 trigger upgrade such as the improvements of algorithms for track finding and muon $p_T$ assignment.

The contribution of the RPC system in the refactored L1 muon trigger architecture is

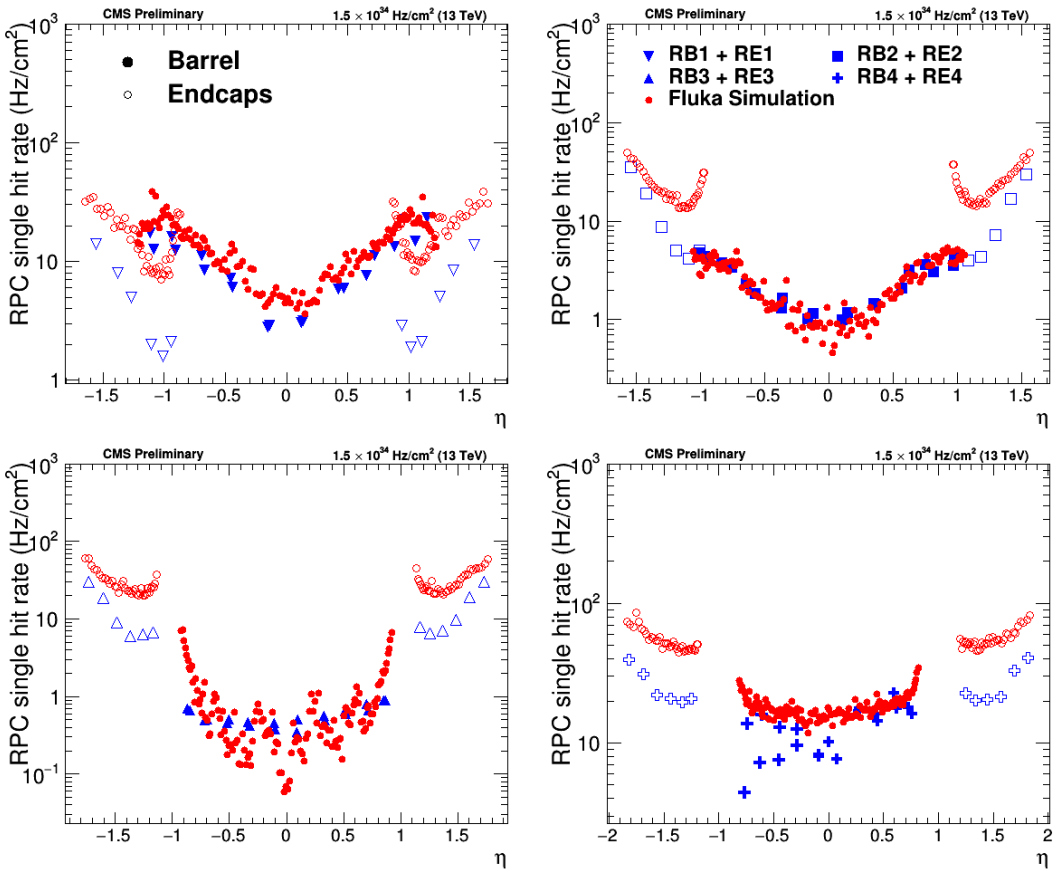


Figure 10: Hit rate as a function of pseudorapidity for the RPC layers is shown (blue) with the results of simulation superimposed (red). The full markers correspond to the barrel layers, while the empy ones - to the endcap. The top plots show the first (on the left) and second (on the right) barrel (RB1 and RB2) and edncap (RE1 and RE2) stations, while the bottom plots describe third and forth barrel (RB3 and RB4) and endcap (RE3 and RE4) stations. Hit rates estimated values were evaluated at $1.5 \times 10^{34}\ cm^{-2}s^{-1}$ instantaneous luminosity and an average over $\phi$ was taken for each layer shown.

different for the three muon track finders and can be summarized as follows.

- BMTF: RPC timing information is used to improve the DT trigger primitives bunch crossing assignment and, in the first two stations (where two RPC layers are present), a segment is built by matching RPC hits from inner and outer chambers in case of DT inefficiency.
- OMTF: since it makes use of both barrel and endcap data, the two above points holds and, in addition to them, RPC hit position is used 'standalone' from the 8 available chambers: 5 in the barrel, 3 in the endcap.
- EMTF: RPC hit position is used in case of CSC trigger primitive absence.

As it is clear from the above, the combination of barrel muon detectors information at early stage allows to exploit the system redundancy already at the step of the trigger primitive building. As shown on the left hand side plot of Fig. 13 [10], this combination brings an average increase of the station 1 barrel trigger primitive efficiency to about 1.4%: from 94.1% (DT only) to 95.5% (DT+RPC). The inefficiencies from one detector being covered by the presence of the other is not the only gain from the new architecture. It also allows to benefit from the detector complementarity as shown on the right plot of Fig. 13, the usage of timing from RPC detector reduces the number of out-of-time DT trigger primitives.

# 7 Conclusions

# References


[1] CMS Collaboration. CMS technical design report, volume II: Physics performance. *J. Phys. G*, 34:995, 2007.

[2] Marcello Abbrescia. Operation, performance and upgrade of the CMS Resistive Plate Chamber system at LHC. *Nucl. Instrum. Meth.*, A732:195–198, 2013.

[3] A. M. Sirunyan et al. Performance of the CMS muon detector and muon reconstruction with proton-proton collisions at $\sqrt{s} = 13$ TeV. *JINST*, 13(06):P06015, 2018.

[4] S Costantini et al. Uniformity and stability of the CMS RPC detector at the LHC. *Journal of Instrumentation*, 8(03):P03017–P03017, 2013.

[5] M.I. Pedraza-Morales, M.A. Shah, and M. Shopova. First results of CMS RPC performance at 13 TeV. *Journal of Instrumentation*, 11(12):C12003–C12003, dec 2016.

[6] S. Costantini, Y. Ban, J. Cai, Q. Li, S. Liu, S. Qian, D. Wang, Z. Xu, F. Zhang, Y. Choi, J. Goh, D. Kim, S. Choi, B. Hong, J.W. Kang, M. Kang, J.H. Kwon, K.S. Lee, S.K. Lee, S.K. Park, L.M. Pant, A.K. Mohanty, R. Chudasama, J.B. Singh, V. Bhatnagar, A. Mehta, R. Kumar, S. Cauwenbergh, A. Cimmino, S. Crucy, A. Fagot, G. Garcia, A. Ocampo, D. Poyraz, S. Salva, F. Thyssen, M. Tytgat, N. Zaganidis, W.V. Doninck, A. Cabrera, L. Chaparro, J.P. Gomez, B. Gomez, J.C. Sanabria, C. Avila, A. Ahmad, S. Muhammad, M. Shoaib, H. Hoorani, I. Awan, I. Ali, W. Ahmed, M.I. Asghar, H. Shahzad, A. Sayed, A. Ibrahim, S. Aly, Y. Assran, A. Radi, T. Elkafrawy, A. Sharma, S. Colafranceschi, M. Abbrescia, C. Calabria, A. Colaleo, G. Iaselli, F. Loddo, M. Maggi, S. Nuzzo, G. Pugliese, R. Radogna, R. Venditti, P. Verwilligen, L. Benussi, S. Bianco, D. Piccolo, P. Paolucci, S. Buontempo, N. Cavallo, M. Merola, F. Fabozzi, O.M. Iorio, A. Braghieri, P. Montagna, C. Riccardi, P. Salvini, P. Vitulo, I. Vai, A. Magnani, A. Dimitrov, L. Litov, B. Pavlov, P. Petkov, A. Aleksandrov, V. Genchev, P. Iaydjiev, M. Rodozov, G. Sultanov, M. Vutova, S. Stoykova, R. Hadjiiska, H.S. Ibargen, M.I.P. Morales, S.C. Bernardino, I. Bagaturia, Z. Tsamalaidze, I. Crotty, and M.S. Kim. Radiation background with the CMS RPCs at the LHC. *Journal of Instrumentation*, 10(05):C05031–C05031, may 2015.

[7] R.I. Rabadan-Trejo, A. Fagot, M. Gul, C. Roskas, M. Tytgat, N. Zaganidis, S. Fonseca De Souza, A. Santoro, F. Torres Da Silva De Araujo, A. Aleksandrov, R. Hadjiiska, P. Iaydjiev, M. Rodozov, M. Shopova, G. Sultanov, A. Dimitrov, L. Litov, B. Pavlov, P. Petkov, A. Petrov, S.J. Qian, D. Han, W. Yi, C. Avila, A. Cabrera, C. Carrillo, M. Segura, S. Aly, Y. Assran, A. Mahrous, A. Mohamed, C. Combaret, M. Gouzevitch, G. Grenier, F. Lagarde, I.B. Laktineh, H. Mathez, L. Mirabito, K. Shchablo, I. Bagaturia, D. Lomidze, I. Lomidze, L.M. Pant, V. Bhatnagar, R. Gupta, R. Kumari, M. Lohan, J.B. Singh, V. Amoozegar, B. Boghrati, H. Ghasemy, S. Malmir, M. Mohammadi Najafabadi, M. Abbrescia, A. Gelmi, G. Iaselli, S. Lezki, G. Pugliese, L. Benussi, S. Bianco, D. Piccolo, F. Primavera, S. Buontempo, A. Crescenzo, G. Galati, F. Fienga, I. Orso, L. Lista, S. Meola, P. Paolucci, E. Voevodina, A. Braghieri, P. Montagna, M. Ressegotti, C. Riccardi, P. Salvini, P. Vitulo, S. W. Cho, S. Y. Choi, B. Hong, K. S. Lee, J. H. Lim, S. K. Park, J. Goh, T. J. Kim, S. Carrillo Moreno, O. Miguel Colin, F. Vazquez Valencia, S. Carpinteyro Bernardino, J. Eysermans, I. Pedraza, C. Uribe Estrada, R. Reyes-Almanza, M.C. Duran-Osuna, M. Ramirez-Garcia, G. Ramirez-Sanchez, A. Sanchez-Hernandez, H. Castilla-Valdez, A. Radi, H. Hoorani, S. Muhammad, M.A. Shah, and I. Crotty. Long-term performance and longevity studies of the CMS resistive plate chambers. *Journal of Instrumentation*, 13(08):P08024–P08024, aug 2018.

[8] A Tapper and Darin Acosta. CMS Technical Design Report for the Level-1 Trigger Upgrade. Technical Report CERN-LHCC-2013-011. CMS-TDR-12, 2013.

[9] CMS Collaboration. Level-1 muon trigger performance in 2017 data and comparison with the legacy muon trigger system. Technical Report CMS-DP-2017-041, 2017.

[10] CMS Collaboration. Performance of the CMS TwinMux Algorithm in late 2016 pp collision runs. Technical Report CMS-DP-2016-074, 2016.

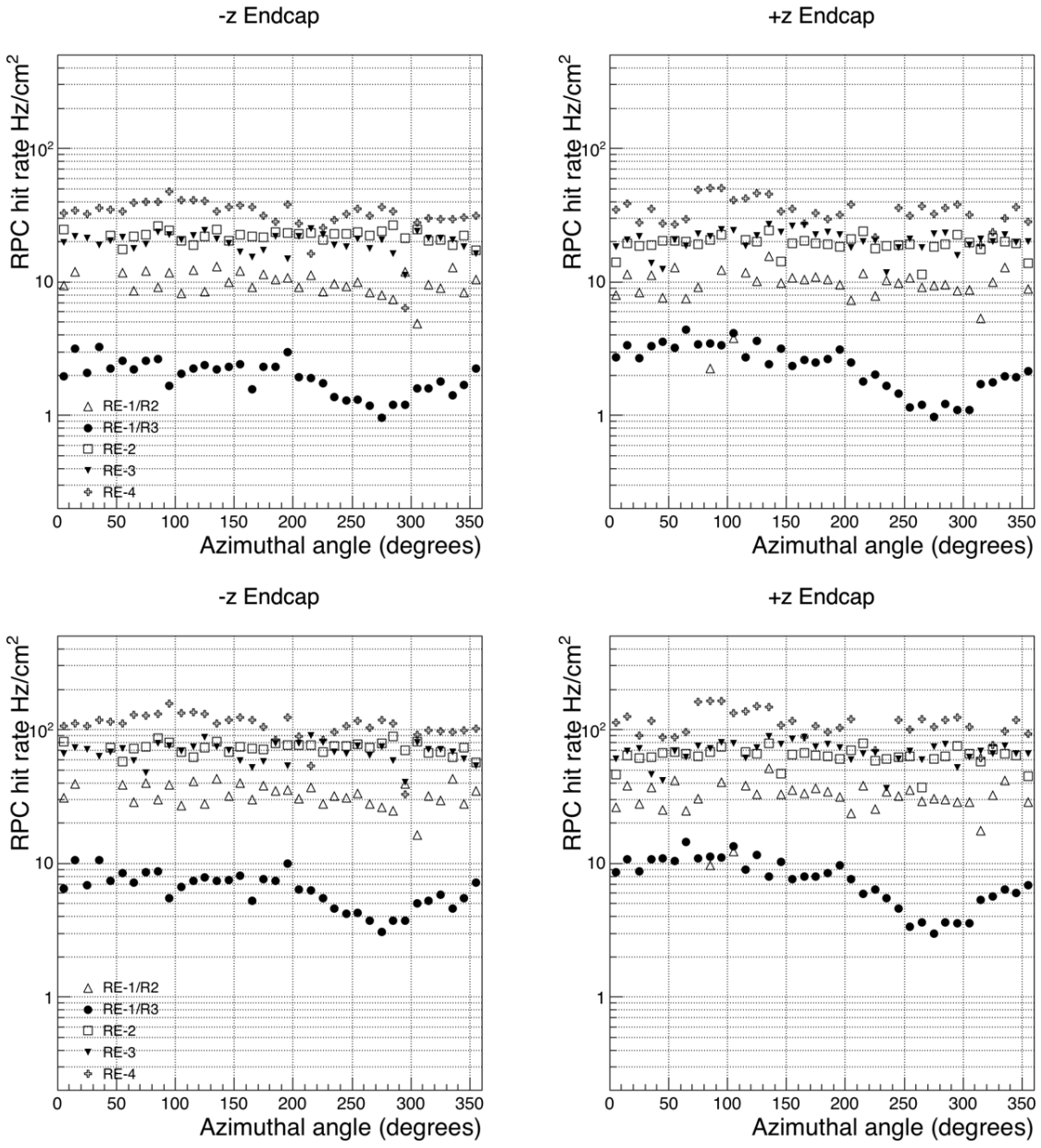


Figure 11: RPC Endcap hit rate $\phi$ distribution for the negative (left) and positive (right) disks. Hit rates evaluated at $1.5 \times 10^{34}\ cm^{-2}s^{-1}$ from the linear dependence on instantaneous luminosity and an average over rings are computed and shown on the top plots. The predicted rates at $5 \times 10^{34}\ cm^{-2}s^{-1}$ are shown on the bottom plots

.

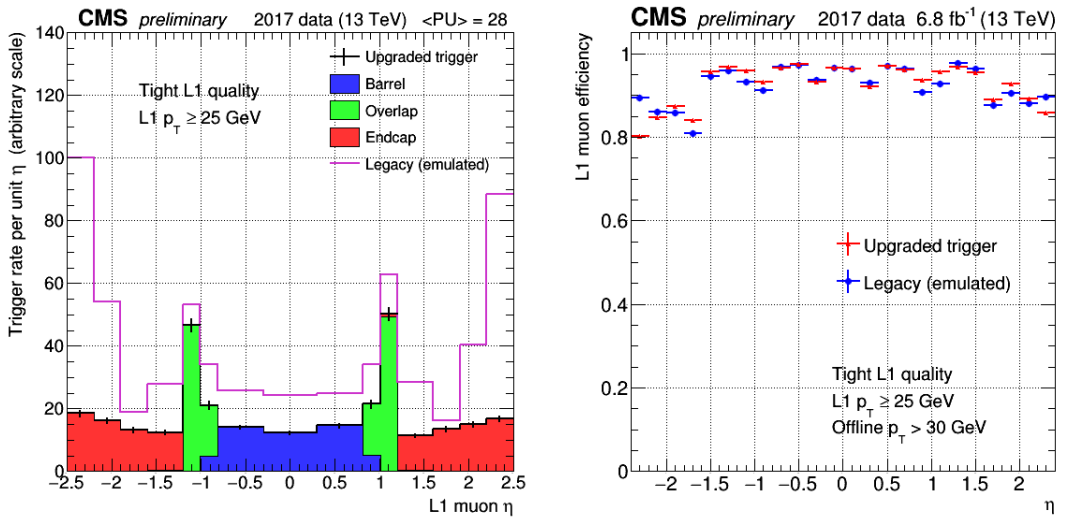


Figure 12: Muon trigger rate (left) and efficiency (right) as a function of pseudo-rapidity, compared between the upgraded (2017) and legacy (2015) systems.

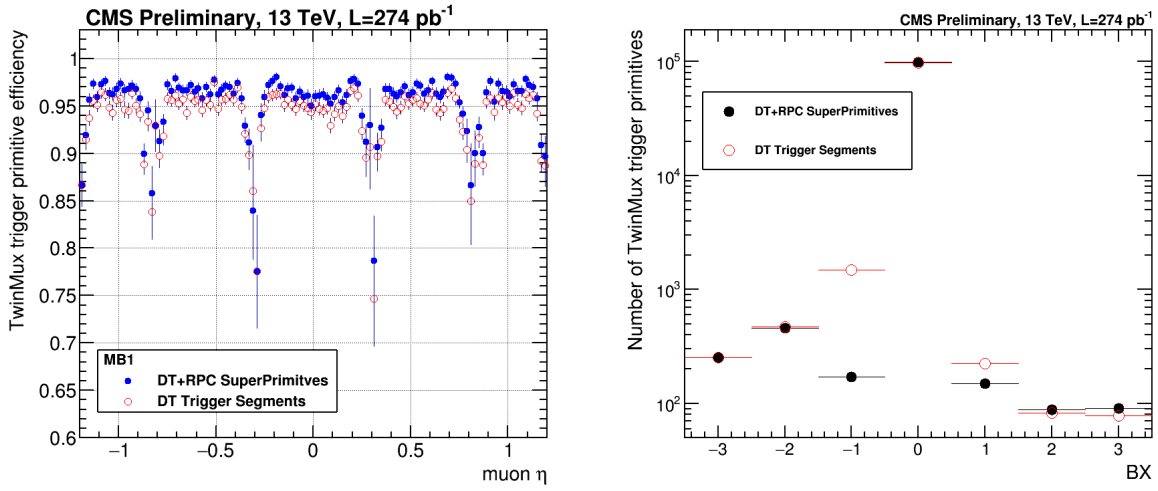


Figure 13: Left: station 1 barrel trigger primitive efficiency as a function of the muon pseudo-rapidity. Right: bunch crossing (BX) distribution of the barrel trigger primitives. The correct event BX is 0.